Mineralogical Magazine, February 1998, Vol. 62(1), pp. 29–40

Melt inclusions in granitoids of the Timna Igneous Complex, Southern Israel

YE. VAPNIK

Department of Geology, Ben-Gurion University of the Negev, P.O. Box 653, Beer-Sheva 84105, Israel

ABSTRACT

High temperature microthermometry and Scanning Electron Microprobe (SEM) analyses were used to study natural magmatic remnants in quartz crystals in granitoids from the Timna Igneous Complex, southern Israel, and to constrain physicochemical parameters during their crystallization. For the porphyritic granite, alkali granite and quartz monzodiorite, liquidus temperatures are 710–770, 770–830 and 770–840°C, respectively; solidus temperatures are 690–770, 710–790 and 770°C, respectively. Pressures during crystallization and water content in the magmas were determined using the phase diagram of the modal granite system. The determined $P-T$-conditions are typical for water-saturated granitoid magmas (>4–8 wt.%) generated and crystallized at a shallow crustal level.

SEM data on melt inclusions support conclusions of previous investigations on two types of granitoid magmas exposed in the Timna Igneous Complex: the porphyritic and alkali granites. Different trends of crystallization are proposed for these granites. Crystallization of the porphyritic granite started with cotectic crystallization of plagioclase and terminated in residual K-feldspar-rich crystallization; crystallization of the alkali granite took place at higher temperatures, starting with K-rich alkali-feldspar crystallization and terminating in residual Na-rich eutectic crystallization.

Parameters not available from other sources — temperature and pressure of the liquidus and solidus stages, water content, trends of crystallization — were obtained for the porphyritic and alkali granites.

KEYWORDS: melt inclusions, granites, porphyritic and alkali, Timna, Israel.

Introduction

MELT inclusions in magmatic minerals preserve unique information on the physicochemical conditions during magma generation and crystallization, including magma composition (Fanggiong-Lu *et al.*, 1995) and volatile content (Bacon *et al.*, 1992). They are well known to occur in rapidly quenched effusive lavas, but may also be present in slowly cooled plutonic rocks; this latter occurrence, however, has been largely ignored, particularly in the western literature (Touret and Frezzotti, 1993). This study describes melt inclusions — or magmatic remnants — in granitoids of the Timna Igneous Complex (TIC), southern Israel. Previous studies concluded that the TIC represents the final stage of evolution of the Precambrian Arabian-Nubian Shield (ANS) (Zlatkine and Wurzburger, 1957; Beyth, 1987; Shpitzer *et al.*, 1992; Beyth *et al.*, 1994*a,b*). The occurrence of melt inclusions in granitoids allow us to take a unique approach to further study the evolution of the TIC and to constrain physical parameters not obtainable from other sources.

An attempt is also made to constrain the volatile content of the magmas that formed the TIC. This effort is complicated by several factors. A small part of the volatiles is trapped as fluid inclusions in quartz; however, these may not be wholly representative of magmatic fluids since commonly a large part of magmatic volatiles escape the system during and after crystallization. Fluid inclusions may be trapped in crystals at any stage of the rock's evolution, further complicating their study. The occurrence of melt inclusions with a small amount of trapped fluid provides an additional opportunity to study magmatic fluids, but the small size of the inclusions (usually up to 15 μm) preclude direct analysis of their fluid fraction. Despite these complications, microthermometric data yield some useful information and help characterize the TIC magmatism.

Geological setting and previous work

The Timna Igneous Complex is exposed at the northern tip of the Arabian-Nubian Shield, in the Timna Valley of southern Israel (Fig. 1). The shield formed during the Pan-African orogenic cycle (*ca.* 900–550 Ma) by the suturing of juvenile arc terrains, followed by magmatic thickening by intrusion of batholiths of predominantly granodiorite composition (Stoeser and Camp, 1985; Stern, 1994). The TIC marks the last stages of the ANS evolution between 625 and 540 Ma (Beyth *et al.*, 1994*a,b*). The intrusive rocks of the TIC consist of five major plutonic and various hypabyssal lithologies (Fig. 1). The plutonic rocks include: (1) olivine norite with up to 40% olivine, 7% orthopyroxene, 15% amphibole and 14% plagioclase and minor pyroxene hornblende peridotite; (2) monzodiorite with 32–38% plagioclase, 5–35% orthoclase and 11–35% amphibole; (3) quartz monzodiorite with 40% plagioclase, 23 % orthoclase, 15% quartz and 3% hornblende; (4) porphyritic granite with 44% plagioclase, 25% orthoclase and 23% quartz; (5) pink alkali granite with 24–57% perthite, 23% orthoclase, 11–25% albite and 22–24% quartz. All the rocks contain biotite. The hypabyssal rocks include dykes of rhyolite, andesite and dolerite, as well as composite andesite-rhyolite dykes (Shpitzer *et al.*, 1992). The age relations among the various plutonic bodies of the TIC are evident from field observations and confirmed by radiometric dating. The porphyritic granite, dated at 625 Ma (Beyth *et al.*, 1994a), is the oldest pluton. It is intruded by alkali granite, olivine norite, and monzodiorite, which are dated at 610 Ma (Beyth *et al.*, 1994*a*). The youngest plutonic rock is the quartz monzodiorite (600 Ma; Beyth and Reichman, 1996) which contains numerous xenoliths of all above mentioned rock types.

The granitoids in the complex have different origins. Whereas the porphyritic granite corresponds to an I-type granitic magma (Beyth, 1987), the alkali granite formed by fractionation from mantle derived monzodiorite and is a marginal A-type granite (Beyth *et al.*, 1994*a*).

Geothermometric calculations based on Al-partitioning between coexisting amphibole and plagioclase, and on the two-feldspar thermometer, indicate temperatures in the range of 500–600°C. Such temperatures are several hundred degrees below solidus temperatures (Shpitzer *et al.*, 1992).

Geobarometry based on Al and Ti contents of amphibole indicates a crystallization pressure of

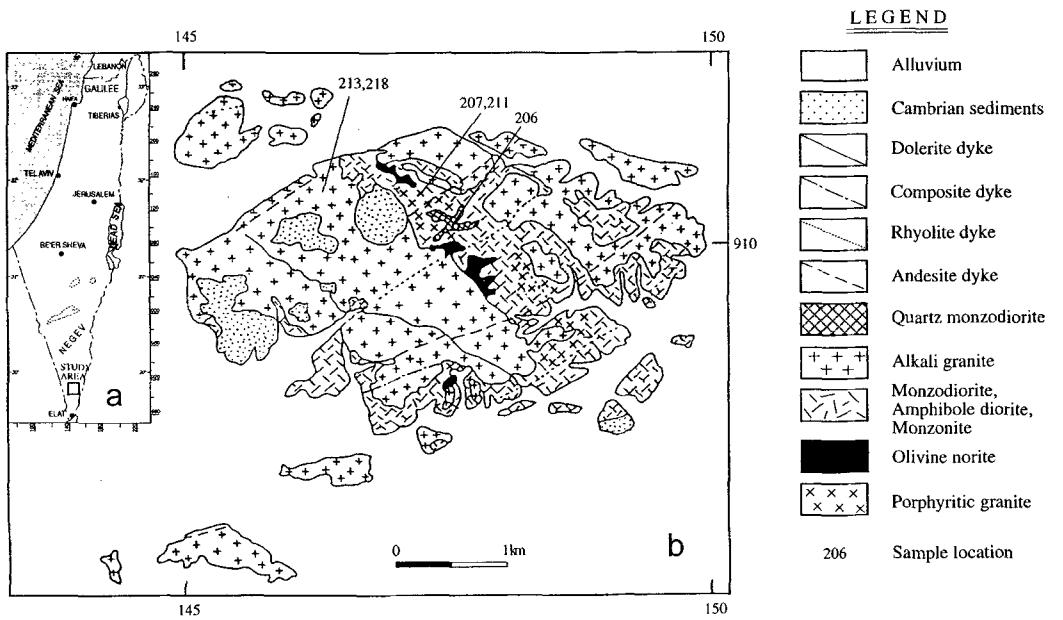

FIG. 1. Geological setting of the Timna Igneous Complex (TIC). (*a*) Map showing location of the TIC in Israel. (*b*) Geological map of the TIC (after Beyth *et al.*, 1994*a*).

less than 5 kbar. The alkali-feldspar phase diagram (McBirney, 1984) suggests that the alkali granite formed at shallow depth (2–5 kbar; Shpitzer *et al.*, 1992). A water pressure of 1–5 kbar is indicated by the CIPW-Qz-Ab-Or diagram (Beyth, 1987).

Melt and fluid inclusion analysis

Sample description

Five samples containing melt and fluid inclusions in quartz were selected for analysis. Figure 2 shows typical occurrences of inclusions. The sample locations are shown in Fig. 1.

Samples 207 and 211 represent the porphyritic granite with orthoclase and microcline phenocrysts. The phenocrysts are up to 2.5 cm in size; matrix minerals are 0.1–0.5 cm. The matrix consists of quartz, biotite, plagioclase, and perthite, with titanite, apatite, and zircon as accessories; sericite and chlorite occur as alteration products (Shpitzer *et al.*, 1992).

Samples 213 and 218 represent the alkali granite. They are composed of orthoclase, perthite and albite, quartz and biotite; apatite and zircon occur as accessories, and sericite and chlorite as alteration products (Shpitzer *et al.*, 1992). The grain size is up to 5 mm.

Sample 206 represents the quartz-monzodiorite. It is composed of plagioclase, orthoclase, quartz, perthite, biotite, and amphibole. The grain size is up to 5 mm.

The whole-rock chemical analyses of major elements in the studied samples are shown in Table 1.

Description of inclusions

The melt inclusions are arranged either as isolated inclusions or as planar arrays and clusters in the quartz crystals. Melt inclusions are numerous in quartz of the porphyritic and alkali granites, but are relatively rare in the quartz-monzodiorite. The melt inclusions are up to 20 μm in size. At room temperature, they contain microcrystalline aggregates ± glass remnants ± one or more gas bubbles. Under the microscope, they have a typical dark and opaque granular aspect. Commonly, melt inclusions have colored glass remnants exhibiting strong anisotropy due to devitrification (Touret and Frezzotti, 1993). Most of the gas bubble became recognizable only after the start of heating experiments (Fig. 2*a*).

Fluid inclusions range in size from 7 to 20 μm. Three generations of fluid inclusions occur in rock-forming quartz grains: primary, secondary and pseudosecondary. The fluid inclusions were categorized as primary, secondary and/or pseudosecondary based on criteria outlined in other fluid inclusion studies of granitoid rocks (e.g. Roedder, 1984). No clear spatial association between melt and fluid inclusions was observed.

Analytical methods

Analyses were made on melt and fluid inclusions occurring in the same samples. Melt inclusions were investigated by high-temperature microthermometry and Scanning Electron Microscopy (SEM) in the following way:

1. Thin sections of rocks were analysed microscopically and by high-temperature micro-

TABLE 1. Major element analysis of granitoids

	Sample 207	211	213	218	206
SiO_2	69.82	70.77	75.63	75.53	66.70
Al_2O_3	16.16	16.45	13.11	13.06	15.78
$FeO+Fe_2O_3$	1.51	1.51	0.91	1.32	3.22
MgO	0.62	0.61	0.22	0.11	1.46
MnO	0.02	0.02	0.03	0.02	0.06
TiO_2	0.26	0.25	0.16	0.16	0.63
Na_2O	5.57	5.67	2.60	3.89	4.70
CaO	2.36	2.21	0.51	0.42	2.54
K_2O	2.25	2.49	6.79	5.48	3.48

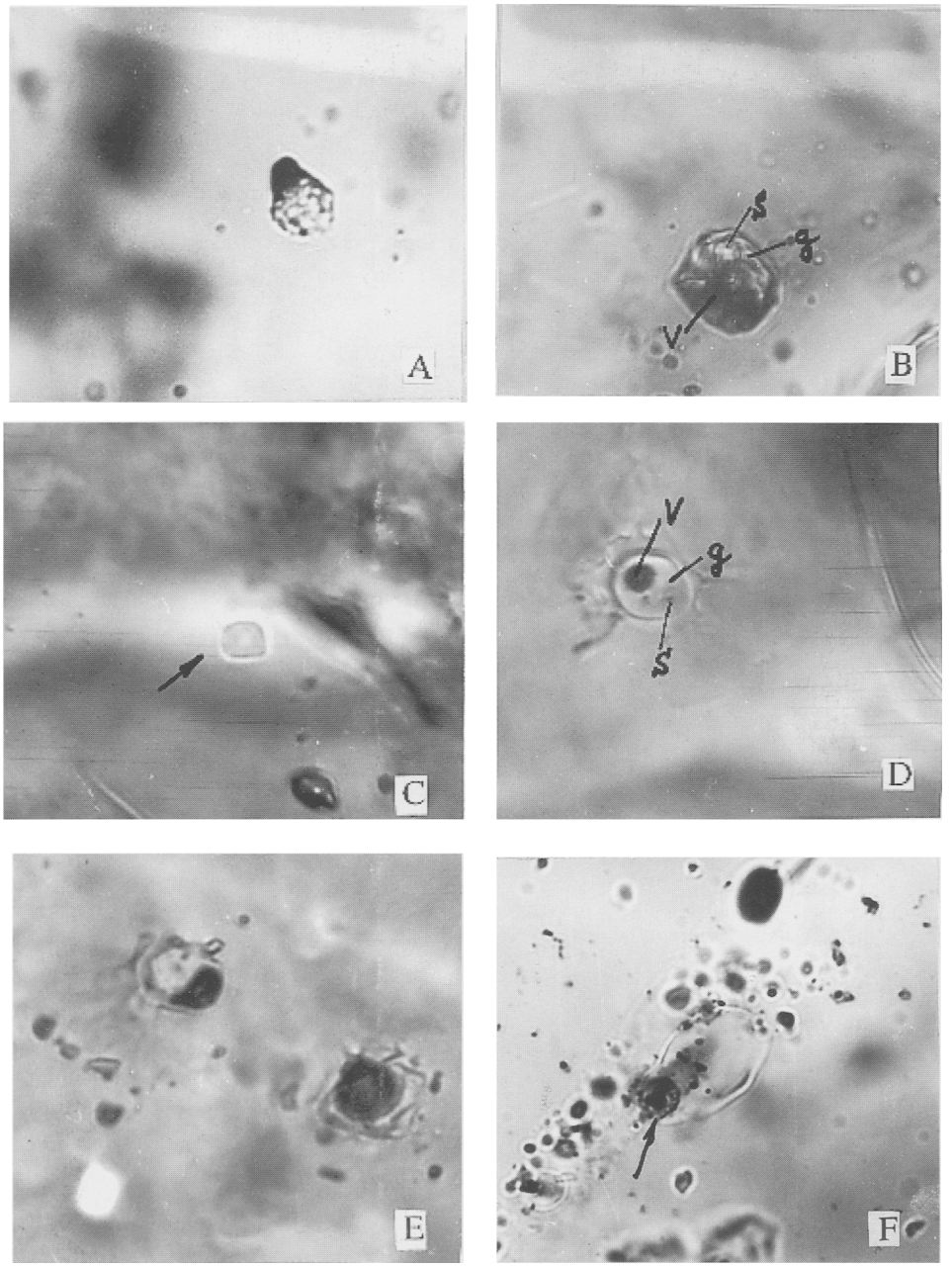

FIG. 2. Melt inclusions in the quartz crystals of the TIC granitoids. (*a*) Sample 218. Melt inclusion (about 10 μm) quenched at 720°C. Melting reaction is started: numerous solid phases, liquid phase (melt) and gas bubble became recognizable in melt inclusion only after heating; (*b*) Sample 218. Melt inclusion (about 20 μm) quenched at 800°C. Melting reaction is in progress: rounded solid phases (s) and black gas phase (v) within the light glass (g) are visible; (*c, d, e*). Sample 207. Melt inclusions of the same cluster quenched at 770°C. Different rates of melting reaction are evident: *c* Completely homogeneous inclusion (indicated by arrow; size about 5 μm); *d* Inclusion (about 15 μm) with black gas phase (v) and small solid phases (s) within glass (g). The homogenization reaction liquid + gas + solid →

thermometry on the heating stage designed by A. Slutsky (Moscow). The heating stage is reliable up to 1650°C and has a very high rate of quenching (several hundred degrees per 10–20 sec) (Keppler and Bagdassarov, 1993; Sobolev *et al.*, 1994). For stage calibration the following melting point standards were used: zinc (419.58°C); a–b phase transformation (573°C); sodium chloride (800.4°C); gold (1064.43°C). Both step-by-step heating and heating-quenching were used. At each temperature step of phase reaction the temperature was held constant for 1–2 hours, thus ensuring complete diffusional equilibrium between silicate melt and coexisting vapour bubbles (Reyf, 1990).

2. After each heating experiment, the melt inclusions were quenched within a time period of 10–20 seconds. Quartz chips containing quenched melt inclusions were ground with 1000 grit silicon carbide powder until the melt inclusions were exposed on the surface, indicated by decrepitation of the gas bubble in the melt inclusion (Fig. 2*f*). The chips were then polished with a 1 μm diamond paste, after which they were cleaned and gold-coated for SEM analysis. The compositions of silicate melt inclusions were analysed by SEM at Ben-Gurion University of the Negev, Department of Applied Research. The SEM analyses covered the vicinity of the decrepitated gas bubble. The scanning beam diameter used was about 1 μm, and accelerating voltage was 20 kV. Standard X-ray detectors were used; therefore elements of atomic weights less than that of Na were not detectable.

The fluid inclusions were studied by microthermometric techniques using a Chaixemeca heating-freezing stage (e.g. Roedder, 1984). The stage was calibrated using the following melting points: CO_2 (−56.6°C); ice (0.0°C); sodium nitrate (306°C); potassium dichromate (398°C).

Results

Melt inclusions

The following temperatures of phase reactions were measured during the heating experiments: (*a*) The temperature of incipient melting, which corresponds to the solidus of the system (Touret and Frezzotti, 1993). At this temperature the melt phase became visible in the inclusion and formed a film on the cavity walls (Fig. 2*a*); (*b*) The temperature of final melting of glass, corresponding to the liquidus of the system (Schiano and Clocchiati, 1994); (*c*) The temperature of gas bubble dissolution and homogenization in the melt. In inclusions trapped during magma boiling, the gas/melt ratios are very variable, and homogenization temperatures (disapearence of the gas bubble) may have no petrological significance (Reyf, 1990; Touret and Frezzotti, 1993).

Three types of melting reactions were observed: (1) solid melting before vapour dissolution (liquid + solid + vapour → liquid + vapour); (2) simultaneous dissolution of solid and vapour (liquid + solid + vapour → liquid); (3) dissolution of the vapour phase preceding complete solid melting (liquid + solid + vapour → liquid + solid → liquid).

Figures 3 and 4 show temperatures of incipient melting in inclusions in the porphyritic granite and the alkali granite, respectively. Measured temperatures range from 690 to 870°C. An incipient melting temperature of about 740°C was determined for only two melt inclusions in a quartz crystal of the quartz-monzodiorite.

The temperatures of final melting of the solid in melt inclusions, according to the three reaction types, are shown for the porphyritic granite and the alkali granite in Figs 5 and 6, respectively. Taken together, the melting data span a range of 700–1060°C. Such a wide range is a known phenomenon for solid phase melting temperatures within a cluster of melt inclusions (Reyf, 1990; Thomas, 1994). The smallest melt inclusions (5–7 μm) had the lowest temperatures of phase transformation and exhibited simultaneous dissolution of the solid phase and gas bubble (second type of melting reaction) (Fig. 2*c,d,e*).

Four liquidus temperatures in the range of 770–840°C were obtained for the quartz monzodiorite. These inclusions show the second type of melting reaction.

---

liquid + gas is nearly complete. Strong reaction rim around melt inclusion is clearly visible; *e* Melt inclusions which are still very far from homogenization (inclusion size 15–20 μm); *f* Sample 218. Melt inclusion (about 15 μm) prepared for SEM analysis. Inclusion is exposed on the surface, as testified by decrepitated gas bubble (indicated by arrow).

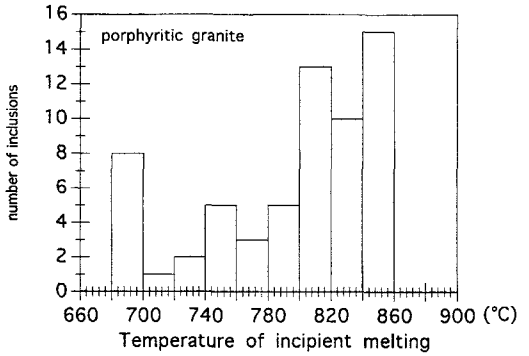

FIG. 3. Temperature of incipient melting (solidus melting) in inclusions in the porphyritic granite. The data are from 62 inclusions in samples 211 and 207.

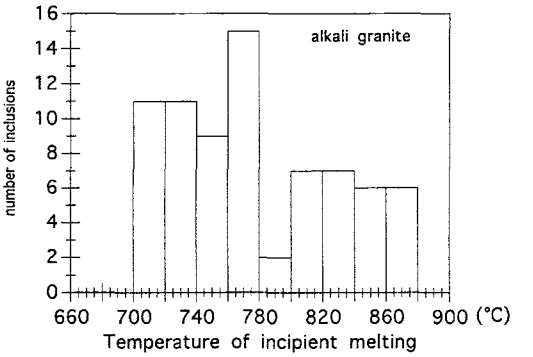

FIG. 4. Temperature of incipient melting (solidus melting) in inclusions in the alkali granite. The data are from 74 inclusions in samples 213 and 218.

The composition of the melt inclusions was determined by SEM analysis of the quenched glass in 20 inclusions (Table 2). SEM analyses show a granitic composition with high silica content (74.70–89.17%). The scatter of the compositional data whithin the same sample is very high. For example, K_2O content ranges from 0.27 to 9.14 (sample 211), and SiO_2 content ranges from 74.88 to 89.17 (sample 218).

The quality of the SEM analyses was checked by comparing the ratios of major elements in melt inclusions in replicate analyses performed at different points within the same inclusion (Table 3). Although the SiO_2 content varies, the K_2O/Na_2O and $Al_2O_3/(K_2O+Na_2O)$ ratios show very good reproducibility.

Analyses of melt inclusions hosted in quartz commonly yield high SiO_2 values (Frezzotti, 1992; Varela, 1994; Vapnik, 1996). This is probably an analytical artifice, reflecting the host mineral's effect on the SEM analyses and partial melting of its cavity walls during the heating experiments (Touret and Frezzotti, 1993; Vapnik, 1996). Although SiO_2 contents may have no petrological significance, the oxide ratios of the other major components may be representative.

Fluid inclusions

Three types of fluid inclusions were identified:

1. Supersaturated brine solution with isotropic and/or anisotropic solid phases. These inclusions are of

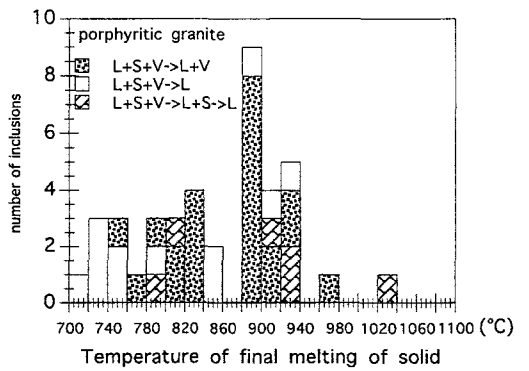

FIG. 5. Temperature of final melting of solid (liquidus temperature) in melt inclusions in the porphyritic granite. The data are from 40 inclusions. Different shading patterns stand for the three types of melting reactions observed.

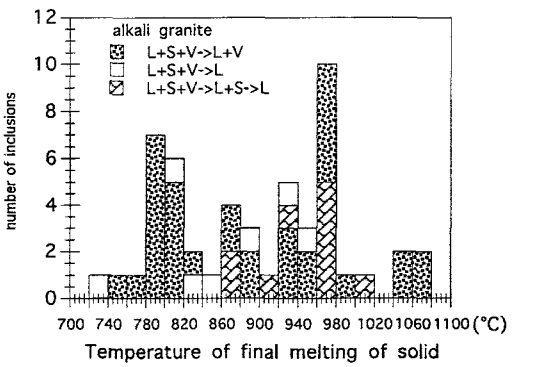

FIG. 6. Temperature of final melting of solid (liquidus temperature) in melt inclusions in the alkali granite. The data are from 52 inclusions. Different shading patterns stand for the three types of melting reactions observed.

TABLE 2. Composition of melt inclusions obtained by SEM analyses of quenched samples

a. Porphyritic granite (sample 211)

SiO_2	77.88	78.07	82.22	74.70
Al_2O_3	12.68	9.13	10.82	14.72
FeO	0.95	0.49	0.24	0.82
MgO		0.00	0.00	0.00
MnO		0.48	0.00	0.42
TiO_2		0.00	0.14	0.08
Na_2O	2.49	1.93	4.15	3.96
CaO		0.76	2.16	0.95
K_2O	6.00	9.14	0.27	4.35

b. Alkali granite (sample 213)

SiO_2	86.15	87.75	79.03	81.57
Al_2O_3	7.64	6.20	11.45	8.91
FeO	0.27	0.60	0.58	0.78
MgO	0.00	0.00	0.07	0.00
MnO	0.16	0.02	0.00	0.00
TiO_2	0.04	0.23	0.00	0.00
Na_2O	2.97	2.04	3.07	2.33
CaO	0.29	0.49	1.20	1.91
K_2O	2.43	2.68	4.60	4.51

c. Alkali granite (sample 218)

SiO_2	83.73	80.53	86.11	78.77	87.95	85.85	84.10	78.88	74.88	86.13	89.17	77.04
Al_2O_3	8.69	8.29	7.61	10.77	6.59	7.23	8.68	11.78	12.01	6.94	4.26	11.01
FeO	0.35	0.66	0.38	1.16	0.23	0.69	0.49	0.77	1.82	0.52	0.15	0.67
MgO	0.00	0.55	0.06	0.00	0.02	0.00	0.00	0.00	0.19	0.08	0.00	0.00
MnO	0.00	0.35	0.00		0.09	0.57	0.09	0.05	0.23	0.14	0.05	0.00
TiO_2	0.09	0.05	0.03	0.16	0.19	0.00	0.31	0.06	0.60	0.00	0.66	0.20
Na_2O	2.72	3.15	1.95	0.99	2.17	1.55	2.04	2.26	1.13	2.16	2.02	4.01
CaO	0.45	1.00	0.25	0.61	0.18	0.18	0.46	1.16	1.50	0.91	0.74	1.06
K_2O	3.96	5.41	3.62	7.55	2.59	3.95	3.83	5.04	7.64	3.11	2.95	6.02

TABLE 3. Comparison of two sets of replicate analyses of melt inclusions (sample 211)

	211 6/11		211 6/12	
SiO_2	78.07	79.86	82.22	88.11
Al_2O_3	9.13	8.14	10.82	6.26
FeO	0.49	0.67	0.24	0.23
MgO	0.00	0.00	0.00	0.00
MnO	0.48	0.26	0.00	0.10
TiO_2	0.00	0.08	0.14	0.00
Na_2O	1.93	2.09	4.15	2.57
CaO	0.76	0.65	2.16	2.58
K_2O	9.14	8.25	0.27	0.16
K_2O/Na_2O	4.74	3.95	0.065	0.062
$Al_2O_3/(K_2O+Na_2O)$	0.82	0.79	2.88	2.29

primary and pseudosecondary origin. During heating at temperatures of about 300°C most inclusions were decrepitated before their complete homogenization. The temperatures of dissolution of the solid phase, which usually follows homogenization of the gas phase, are in the range of 340°C to more than 520°C. The salinity of super saturated fluid inclusions is in the range 40 →55 eq. wt.% NaCl (Roedder, 1984).

2. Fluid inclusions with initial melting temperature in the range of −23 to −11°C and final melting of ice in the range of −20 to −2°C. These are mainly NaCl solutions (Borisenko, 1982) with salinity up to 22 eq. wt.% NaCl (Potter *et al.*, 1978). These inclusions were found in pseudosecondary trails.

3. Low-salinity fluid inclusions with final temperature of ice melting in the range of −5.5

to −1.0°C. These inclusions with salinity up to 8 eq. wt.% NaCl (Potter *et al.*, 1978) form pseudosecondary and secondary trails.

CO_2 inclusions and/or other gases were not identified in the samples studied.

Discussion

Magmatic and meteoric fluids

Fluid-inclusion data can be used to characterize the composition of the fluid phase participating in the granite formation. A fluid in equilibrium with crystallizing granite magmas must be enriched in salt and gases that have low solubility in the melt phase (mainly CO_2, CH_4 and N_2) (Roedder, 1984; Frezzotti, 1992). The TIC granitoid samples contain only supersaturated primary brine inclusions (the first type) and no gases. Inclusion homogenization occurs by halite dissolution and varies from 340 to >520°C; at temperatures higher than 300°C most inclusions are decrepitated. These data suggest a progressive fluid exsolution from crystalizing granitoids. The second type of lower salinity, undersaturated fluid inclusions may reflect the fluid composition during the last stages of granitoid crystallization, when continued fluid exsolution from the granite has resulted in gradually decreasing salinity (Harris, 1986). It is therefore likely that the primary fluid consists mainly of an NaCl-rich solution without CO_2 or other gases with low solubility in the melt. This conclusion agrees with the empirical observation that granites formed and/or emplaced near the surface tend to be H_2O-rich and CO_2-poor, whereas CO_2 is very abundant in lower crustal magmas (Touret, 1987). The very low-salinity inclusions (the third type) are probably related to meteoric water infiltration.

Interpretation of high-temperature thermometric data

The thermometric characteristics of the melt inclusions (Figs 3, 4, 5 and 6) are very dependent on the inclusion size. Only a few inclusions from each sample show low temperature for the incipient melting (Figs 3 and 4), melting of solid (Figs 5 and 6) and dissolution of the gas phase. Most of these low-temperature inclusions are also the smallest (up to 5−7 μm). In contrast, the biggest inclusions (commonly about 20 μm) yield temperatures that are usually unreasonably high (up to 900 → 1000°C) for melt inclusions hosted in granitoids.

Several studies have reported both low-temperature and high-temperature phase reactions in melt inclusions (Takenouchi and Imai, 1975; Reyf, 1990; Naumov *et al.*, 1993; Schiano and Clocchiatti, 1994; Varela, 1994). This common observation may partly reflect experimental procedures. During heating experiments, temperatures must be held constant for long periods of time (from 1 to over 3 hours) in order to achieve equilibrium (Thomas, 1994). Large inclusions require longer experiment durations. Reyf (1990) argues that high-temperature melt inclusion characteristics are related to partial decrepitation of melt inclusions during heating experiments. For the purposes of geothermometry, this implies that only minimum temperatures obtained are significant.

Accordingly, in this study, only a small part of melt inclusions — mostly the smallest ones yielding the lowest-temperature data are used to determine solidus and liquidus temperatures for the TIC granitoids. Figure 7 compares data on inclusions from the porphyritic and alkali granites. It is evident that the alkali granite magma formed at a higher temperature. Solidus temperatures of melt inclusions in the porphyritic and alkali granites are nearly the same, whereas liquidus temperatures are higher for the alkali granite.

Volatile content of the magmas

The microthermometric data indicate that, at the liquidus, the magmas were saturated with volatiles (Figs. 5 and 6): nearly all the low-temperature melt inclusions show the vapour-saturated melting reactions liquid + solid + vapour → liquid + vapour or liquid + solid + vapour → liquid.

Figure 8 shows the phase diagram for the granite system in Pressure-Temperature space with isopleths of water solubility in the melt (Reyf, 1990). The diagram was constructed using experimental data and estimates (Kadik *et al.*, 1971; Ryabchikov, 1975; Piwinskii, 1968; Stern *et al.*, 1975; Tuttle and Bowen, 1958) and is in good agreement with the newly published data on granitic melts (Holtz and Johannes, 1994). To a first approximation this diagram can be applied to the studied TIC granites.

Table 4 summarizes the physicochemical parameters for the magmas, as determined from Fig. 8. The water content and pressures at the liquidus stage are determined from the invariant point in the graph where the melting reaction liquid + solid + vapour → liquid intesects the liquidus curve. The use of the water-saturated

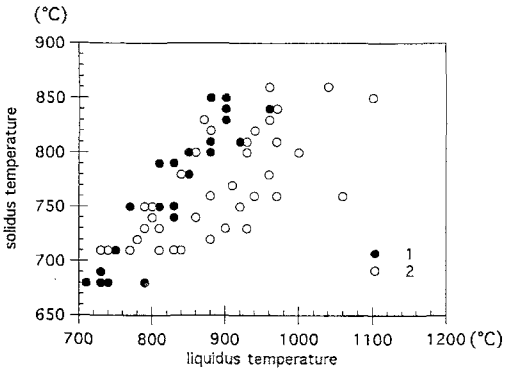

FIG. 7. Solidus *vs* liquidus temperatures of melt inclusions. 1 — data on melt inclusions in the porphyritic granite; 2 — data on melt inclusions in the alkali granite.

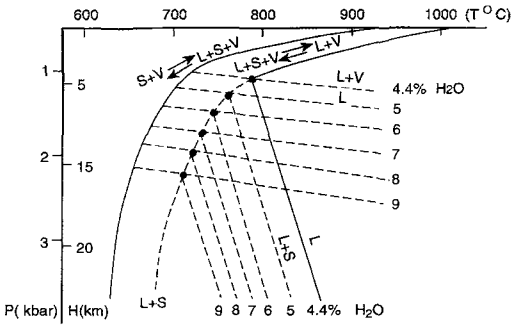

FIG. 8. Phase diagram of the model granite system (Reyf, 1990). The invariant points discussed in text are shown.

curves to determine water content is justified because the fluid inclusion data indicate that water was the dominant fluid during magma crystallization.

The pressures at the solidus stage are determined from the intersections of incipient melting temperatures of the melt inclusions and the water-saturated solidus curve.

Granite magmas chemistry

The chemical evolution of the magmas is difficult to interpret from melt inclusion data. Melt inclusions in crystals represent the magma composition at an unknown time in its evolution (Hansteen and Lustenhouwer, 1990; Frezzotti, 1992: Varela, 1994). SEM analyses of melt inclusions are commonly enriched in SiO_2 due to contamination by the host quartz during analysis; thus the data cannot be examined in the commonly used Quartz-Albite-Orhtoclase (Qz-Ab-Or) diagram. Therefore, major element ratios rather than absolute values are used to analyse the data.

Figures 9 and 10 show graphs of $Al_2O_3/(K_2O+Na_2O)$ *vs* $K_2O/(K_2O+Na_2O)$ atomic ratios for melt inclusions, whole rock (Beyth *et al.*, 1994*a*), and Na- and K-feldspars in granitoids (Shpitzer *et al.*, 1992).

SEM analyses of melt inclusions in the porphyritic granite (Fig. 9) show a negative relation between $Al_2O_3/(K_2O+Na_2O)$ and $K_2O/(K_2O+Na_2O)$ where high $Al_2O_3/(K_2O+Na_2O)$ ratios are related to plagioclase (oligoclase) and high $K_2O/(K_2O+Na_2O)$ ratios are related to K-

TABLE 4. Pressure-Temperature conditions and water content at liquidus and solidus of granitoid magmas

	Porphyritic granite (625 Ma)	Alkali granite (610 Ma)	Quartz-monzodiorite (600 Ma)
Liquidus stage			
temperature (°C)	710–770	770–830	770–840
pressure (kbar)	3.2–1.5	1.5–1.0	1.5
depth (km)	10.5–5.0	5.0–3.5	5.0
Water content (wt.%)	8–5	5–4	5–4
Solidus stage			
temperature (°C)	690–700	710–790	770
pressure (kbar)	1.5–1.0	1.0–0.5	0.5
depth (km)	5.0–3.5	3.5–1.7	1.7

feldspar. Thus, the plagioclase and K-feldspar compositions are in good agreement with the SEM data on the extreme left and the extreme right of Fig. 9, respectively. Hence the melt inclusions with a high $Al_2O_3/(K_2O+Na_2O)$ ratio and low $K_2O/(K_2O+Na_2O)$ ratio reflect plagioclase crystallization, whereas the melt inclusions with low $Al_2O_3/(K_2O+Na_2O)$ ratios and high $K_2O/(K_2O+Na_2O)$ ratios correspond to crystallization of K-feldspar-rich composition.

SEM analyses of melt inclusions in the alkali granite (Fig. 10) show variable $K_2O/(K_2O+Na_2O)$ ratios but rather constant $Al_2O_3/(K_2O+Na_2O)$ ratio. This may indicate a crystallization of differently composed alkali feldspar. The analyses on the extreme right of Fig. 10 are in a good agreement with K-rich alkali feldspar composition, whereas analyses on the extreme left reflect Na-rich alkali feldspar.

Figure 11 shows data for samples 211, 213, and 218 plotted on a Qz-Ab-Or diagram. The porphyritic and alkali granites occupy the albite-rich and orthoclase rich fields, respectively. Thus, crystallization of the porphyritic granite must have started with the cotectic plagioclase crystallization and terminated in residual K-feldspar-rich crystallization, whereas crystallization of the alkali granite must have followed the opposite trend, beginning with cotectic alkali-feldspar crystallization and terminating in residual Na-feldspar-rich eutectic crystallization.

Character of crystallization

The presence of fluid inclusions with different salinities may reflect a gradual decrease in fluid salinity during progressive fluid exsolution from a crystallizing magma. Fluid exsolution apparently occured without boiling, as indicated by the absence of coexisting brine-rich and vapour-rich inclusions. This phenomenon may reflect slow crystallization and differentiation of the magma, an interpretation that is supported by the SEM melt inclusion data.

Petrological implication

The obtained high $K_2O/(K_2O+Na_2O)$ and K_2O/Na_2O ratios in the melt inclusions of the porphyritic granite are petrologically significant. They are neither an analytical mistake (Table 3) nor an accidental phenomenon. The generation of potassium-rich silica-saturated rocks, termed ongonite (Le Maitre, 1989), is controversial (Stewart, 1979; Sutherland, 1982; Nockolds *et al.*, 1978). The high K_2O content in melt inclusions indicates the possibility of ongonite magmatic origin (Kovalenko and Kovalenko, 1976) due to differentiation of ordinary water-saturated granite magma. Such magma differentiation may have occured on a bigger scale in the Elat area. The potassium-rich rhyolite dyke in the Nahal Shlomo area (Vapnik, 1996) may also be related to this process.

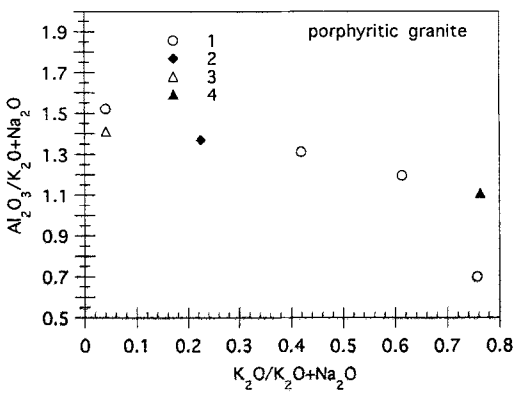

FIG. 9. $Al_2O_3/(K_2O+Na_2O)$ *vs* $K_2O/(K_2O+Na_2O)$ ratios in melt inclusions in the porphyritic granite (sample 211). 1 — SEM data on melt inclusions; 2 — whole rock composition (Beyth *et al.*, 1994a); 3 — plagioclase composition (Shpitzer *et al.*, 1992); 4 — K-feldspar compositions (Shpitzer *et al.*, 1992).

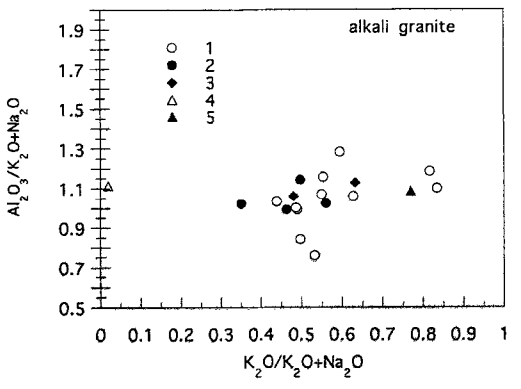

FIG. 10. $Al_2O_3/(K_2O+Na_2O)$ K2O/K2O+Na2O ratios in melt inclusions in the alkali granite (samples 213 and 218). 1 — SEM data on melt inclusions in sample 218; 2 — SEM data on melt inclusions in sample 213; 3 — whole rock composition (Beyth *et al.*, 1994*a*); 4 — albite compositions (Shpitzer *et al.*, 1992); 5 — alkali-feldspar compositions (Shpitzer *et al.*, 1992).

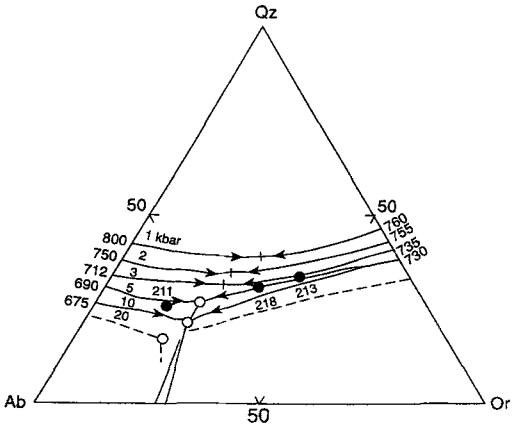

FIG. 11. Whole rock chemical analyses of the porphyritic (sample 211) and alkali (samples 213, 218) granites (Beyth *et al.*, 1994*a*) in the system Qz-Ab-Or-H_2O. 1, 2, 3, 5 10 and 20 kbar are H_2O-saturated liquidus $P-T$-field boundaries for various water pressure (after Johannes, 1985).

Conclusion

Melt inclusions in the granitoids of the TIC are remnants representing the magmatic stage of granite formation. A microthermometric investigation of the melt inclusions reveals the $P-T$-conditions of magma genesis. The temperature and pressure data are typical for water-saturated granitic magmas generated and crystallized at shallow crustal levels. An overall tendency of pressure decrease from the oldest porphyritic granite to the youngest quartz-monzodiorite is evident (Table 4).

The granitic magmas had high initial water content (>4–8 wt.%). Such a high water content is typical for ore-bearing granitoid magmas (Reyf, 1990).

Fluid inclusion data shed light on the fluid composition and the dynamics of granite magma crystallization. During exsolution, the fluid consisted of a relatively saline NaCl solution.

Although SEM analyses of melt inclusions show very high SiO_2 content, they have good reproducibility. The ratios of other major elements (Al, K, Na) can be used to characterize magma content and the dynamics of crystallization.

Geological and geochemical data point to two types of granitic magmas in the TIC: porphyritic and alkali. These data are further supported by the composition of melt inclusions. Crystallization of the porphyritic granite started with cotectic crystallization of plagioclase and terminated in residual K-feldspar-rich crystallization. Crystallization of the alkali granite took place at higher temperature, starting with crystallization of K-rich alkali-feldspar and terminating in residual Na-rich eutectic crystallization.

Acknowledgements

I am thankful to Dr M. Beyth, who provided the samples used for this study and critically discussed the data. This study also benefitted from stimulating discussions with Dr V. Samoylov, who gave me some general trends of thoughts. The article was greatly improved by an anonymous reviewer.

References

Bacon, C.R., Newman, S. and Stolper, E. (1992) Water, CO_2, Cl, and F in melt inclusions in phenocrysts from the Holocene explosive eruptions, Crater Lake, Oregon. *Amer. Mineral.*, **77**, 1021–30.

Beyth, M. (1987) The Precambrian magmatic rocks of Timna Valley, southern Israel. *Precambrian Research*, **36**, 21–38.

Beyth, M. and Reichman, T. (1996) The age of the quartz monzodiorite, the youngest plutonic intrusion in the Timna Igneous Complex. *Isr. Geol. Soc. Annual Meeting*, 13.

Beyth M., Stern, R.J., Altherr, R. and Kroner, A. (1994*a*) The Late Precambrian Timna igneous complex, Southern Israel: Evidence for comagmatic-type sanukitoid monzodiorite and alkali granite magma. *Lithos*, **31**, 103–24.

Beyth, M., Stern, R.J., Alther, R., Peltz, S. and Heimann, A. (1994*b*) Petrochemistry of doleritic dykes from Mount Timna, southern Israel: implications for plate tectonic setting. *Geol. Surv. Isr. Curr. Res.*, **9**, 24–6.

Borisenko, A.S. (1982) Analysis of the salt composition of gas-liquid inclusions in minerals with the help of cryometrical method. In *Application of Thermobarogeochemical Methods for Prospecting and Study of Ore Deposits*. Moscow, Nedra, 37–46 (in Russian).

Fanggiong-Lu, Anderson, A.T. and Davis, A.M. (1995) Diffusional gradients at the crystal/melt interface and their effect on the composition of melt inclusions. *J. Geol.*, **105**, 591–7.

Frezzotti, M.L. (1992) Magmatic immiscibility and fluid phase evolution in the Mount Genis granite (southeastern Sardinia, Italy). *Geochim. Cosmochim. Acta*, **56**, 21–33.

Hansteen, T.H. and Lustenhouwer, W.J. (1990) Silicate

melt inclusions from a mildly peralkaline granite in the Oslo paleorift, Norway. *Mineral. Mag.*, **54**, 195–205.

Harris, C. (1986) A quantitative study of magmatic inclusions in the plutonic ejecta of Ascension Island. *J. Petrol.*, **27**, 251–76.

Holtz, F. and Johannes, M. (1994) Maximum and minimum water contents of granitic melts: implications for chemical and physical properties of ascending magmas. *Lithos*, **32**, 149–59.

Johannes, W. (1985) The significance of experimental studies for the formation of migmatites. In *Migmatites* (J.R. Ashworth, ed.), Blackie and Son Ltd, 36–85.

Kadik, A.A., Lebedev, E.B. and Khitarov, N.I. (1971) *Water in Magmatic Melts*. Moscow, Nauka, 265 pp. (in Russian).

Keppler, H. and Bagdassarov, N.S. (1993) High-temperature FTIR spectra of H_2O in rhyolite melt to 1300°C. *Amer. Mineral.*, **78**, 1325–8.

Kovalenko, V.I. and Kovalenko, N.I. (1976) *Ongonites (topaz-bearing quartz keratophyre) - subvolcanic analogue of rare-metal Li-F granites.* Moscow, Nauka, 108 pp. (in Russian).

Le Maitre, R.W., ed. (1989) *A Classification of Igneous Rocks and Glossary of Terms. Recommendations of the International Union of Geological Sciences Subcomission of the Systematics of Igneous Rocks.* Blackwell, 193 pp.

McBirney, A. (1984) *Igneous Petrology*. San Francisco, Freeman, Cooper and Co., 504 pp.

Naumov, V.B., Solovova, I.P., Kovalenker, V.A. and Rusinov, V.L. (1993) Immiscibility in acidic magmas: Evidence from melt inclusions in quartz phenocrysts of ignimbrites. *Eur. J. Mineral.*, **5**, 937–41.

Nockolds, S.R., Knox, R.W.O.B. and Chinner, G.A. (1978) *Petrology for Students*. Cambridge Univ. Press. 435 pp.

Piwinskii, A.J. (1968) Experimental studies of igneous rock series, Central Sierra Nevada Batholith, California. *J. Geol.*, **78**, 548–70.

Potter, R.W. II, Clynne, M.A. and Brown, D.L. (1978) Freezing point depression of aqueous sodium chloride solutions. *Econ. Geol.*, **73**, 284–5.

Reyf, F.G. (1990) *Ore Potential of Granites and Conditions of its Realization.* Moscow, Nauka, 181 pp. (in Russian).

Roedder, E. (1984) *Fluid inclusions. Reviews in Mineralogy*, 644 pp.

Ryabchikov, I.D. (1975) *Thermodynamics of Fluid Phase of Granitoid Magmas*. Moscow, Nayka, 232 pp. (in Russian).

Schiano, P., and Clocchiatti, R. (1994) World wide occurrence of silica-rich melts in sub-continental and sub-oceanic mantle minerals. *Nature*, **368**, 621–4.

Shpitzer, M., Beyth, M. and Matthews, A. (1992) Igneous differentiation in the Late Precambrian plutonic rocks of Mt. Timna. *Isr. J. Earth Sci.*, **40**, 17–27.

Sobolev, A.V., Gurenko, A.A. and Shimizu, N. (1994) Ultra-depleted melts from Iceland: data from melt inclusion studies. *Mineral. Mag.*, **58A**, 860–1.

Stern, R. J. (1994) Arc assembly and continental collision in the Neoproterozoic East African Orogen: Implications for consolidation of Gondwanaland. *Annu. Rev. Earth. Sci.*, **22**, 319–51.

Stern, C.R., Huang, W.-L. and Wyllie, P.J. (1975) Basalt-andesite-rhyolite-H_2O: crystallization intervals with excess H_2O and H_2O-undersaturated liquidus surfaces to 35 kilobars, with implications for magma genesis. *Earth Planet. Sci. Lett.*, **28**, 189–96.

Stewart , D.B. (1979) The formation of siliceous potassic glassy rocks. In: *The Evolution of the Igneous Rocks*. (H.S. Yoder, Jr, ed.) Princeton University Press, Princeton, 339–50.

Stoeser, D.B. and Camp, V.E. (1985). Pan-African microplate accretion of the Arabian Shield. *Geol. Soc. Amer. Bull.*, **96**, 817–26.

Sutherland, D.S., ed. (1982) *Igneous Rocks of the British Isles*. Wiley & Sons, 645 pp.

Takenouchi, S. and Imai, H. (1975) Glass and fluid inclusions in acidic igneous rocks from some mining areas in Japan. *Econ. Geol.*, **70**, 750–69.

Thomas, R. (1994) Estimation of the viscosity and the water content of silicate melts from melt inclusion data. *Eur. J. Mineral.*, **6**, 511–35.

Touret, J.L.R. (1987) Fluid distribution in the continental lithosphere. In: *Proterozoic Lithospheric Evolution.* (A. Kroner, ed.) Amer. Geoph. Univ. 27–33.

Touret, J.L.R. and Frezzotti, M.L. (1993) Magmatic remnants in plutonic rocks. *Bull. Soc. geol. France*, **164**, 229–42.

Tuttle, O.F. and Bowen, N.L. (1958) Origin of granite in the light of experimental studies in the system $NaAlSi_3O_8$-$KAlSi_3O_8$-H_2O. *Geol. Soc. Amer. Mem.*, **74**, 1–153.

Vapnik, Ye. (1996) Melt inclusions in a dyke of peralkaline rhyolite (Nahal Shlomo area, Southern Israel). *Neues Jahrb. Miner., Mh.*, 365–76.

Varela, M.E. (1994) Silicate-melt and fluid inclusions in rhyolitic dykes, Los Manantiales mining district, Argentina. *Eur. J. Mineral.*, **6**, 837–54.

Zlatkine, A. and Wurzburger, U. (1957) Eruptive rocks of Timna (Negev). *Geol. Surv. Isr. Bull.*, **14**, 41 pp.

[*Manuscript received 9 January 1997: revised 10 June 1997*]